ACS OMEGA

Article

http://pubs.acs.org/journal/acsodf

Noncrystalline Titanium Oxide Catalysts for Electrochemical Oxygen Reduction Reactions

Satoshi Tominaka,*[,†] Akimitsu Ishihara,*[,‡] Takaaki Nagai,[§] and Ken-ichiro Ota[§]

[†]International Center for Materials Nanoarchitectonics (MANA), National Institute for Materials Science (NIMS), 1-1 Namiki, Tsukuba, Ibaraki 305-0044, Japan

[‡]Institute of Advanced Sciences and [§]Green Hydrogen Research Center, Yokohama National University, 79-5 Tokiwadai, Hodogaya-ku, Yokohama, Kanagawa 240-8501, Japan

Supporting Information

ABSTRACT: Titanium oxides crystals are widely used in a variety of fields, but little has been reported on the functionalities of noncrystalline intermediates formed in their structural transformation. We measured the oxygen reduction reaction activity of titanium oxide nanoparticles heat-treated for a different time and found that the activity abruptly increased at a certain time of the treatment. We analyzed their structures by using X-ray pair distribution functions with the help of high-resolution transmission electron microscopy and X-ray photoelectron spectroscopy and ascertained that the abrupt increase in the activity corresponded to a structural transformation from a reduced lepidocrocite-type layered titanate to a disordered structure consisting of domains of brookite-like TiO_6 octahedral linkages. The further treatment transformed these brookite-like domains into another phase having more edge-sharing sites like the TiO-type cubic structure. This finding would position noncrystalline, disordered structure as a possible origin of the catalytic activity, though nanocrystalline rutile particles might be also considered as the origin.

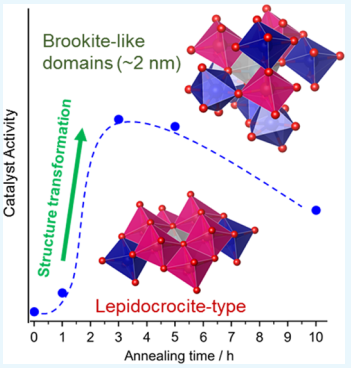

INTRODUCTION

Titanium oxides are used in a variety of fields because of their functionalities, abundance, and environmental friendliness; especially, titanium dioxide crystals (rutile, anatase, brookite, etc.) are mostly used for catalysis applications. Titanium oxides adopt diverse structures, including the polymorphs of titanium dioxide mentioned above, and show structural transformation upon thermal treatment or oxidation/reduction treatment.[1] The structures are, in general, composed of TiO_6 octahedra forming three/two-dimensional networks.[2] For example, brookite, anatase, and rutile are composed of edge-sharing and corner-sharing TiO_6 linkages to form three-dimensional crystal structures.

Compared with such crystalline phases, little has been reported on noncrystalline or disordered intermediates formed during the structural transformation, though they might have unique coordination environments.[3,4] Regarding the structure formation of titanium dioxide crystals in solvothermal reactions, the noncrystalline lepidocrocite-type layered titanate was found to be a common intermediate.[5] Titanium oxides adopt a variety of structures, and thus such intermediates may be diverse as well and indeed important for understanding the structural transformation.[5−7] Moreover, the functionalities of such noncrystalline phases were less investigated, and are interesting for creating new properties.

Here, we show that a titanium oxide nanoparticle system exhibits an abrupt increase of the catalytic activity associated with the formation of an intermediate, noncrystalline structure during the structural transformation between lepidocrocite-type titanate and rutile structure. Titanium oxide crystals (rutile TiO_2, anatase TiO_2, corundum Ti_2O_3, etc.) have been investigated as the potential electrocatalysts for the electrochemical oxygen reduction reactions (ORR),[8−13] but it was found that a noncrystalline intermediate phase could be active in the reactions. Thus, we have investigated the relationship between their structures and activities systematically.

EXPERIMENTAL SECTION

Synthetic Procedures. The catalysts were synthesized by the thermal decomposition of oxytitanium tetrapyrazinoporphyrazine (TiOTPPz) on multiwalled carbon nanotubes as reported previously.[9,14] In brief, TiOTPPz was mixed with carbon nanotubes, (i) heated up to 900 °C in Ar, (ii) retained at the temperature in Ar containing 2% H_2 and 0.05% O_2, where equilibrium O_2 partial is 1.3×10^{-19} atm (retention time = 0, 0.5, 1, 3, 5, and 10 h), and then (iii) cooled down to room temperature. To investigate the contribution of the carbon materials to the catalytic reactions, the samples without oxides were prepared by removing the oxides with hydrofluoric acid.

The contents of the titanium oxides were determined by calcination in dry air up to 1000 °C; 8.0 (0 h), 9.3 (0.5 h), 9.3 (1 h), 9.6 (3 h), 10.7 (4 h), and 16.6 (10 h) wt %. We revealed that this slight increase in the loading amount was attributable to the partial pyrolysis of carbons through the thermogravi-

Received: June 18, 2017
Accepted: August 16, 2017
Published: August 30, 2017

DOI: 10.1021/acsomega.7b00811
ACS Omega 2017, 2, 5209−5214

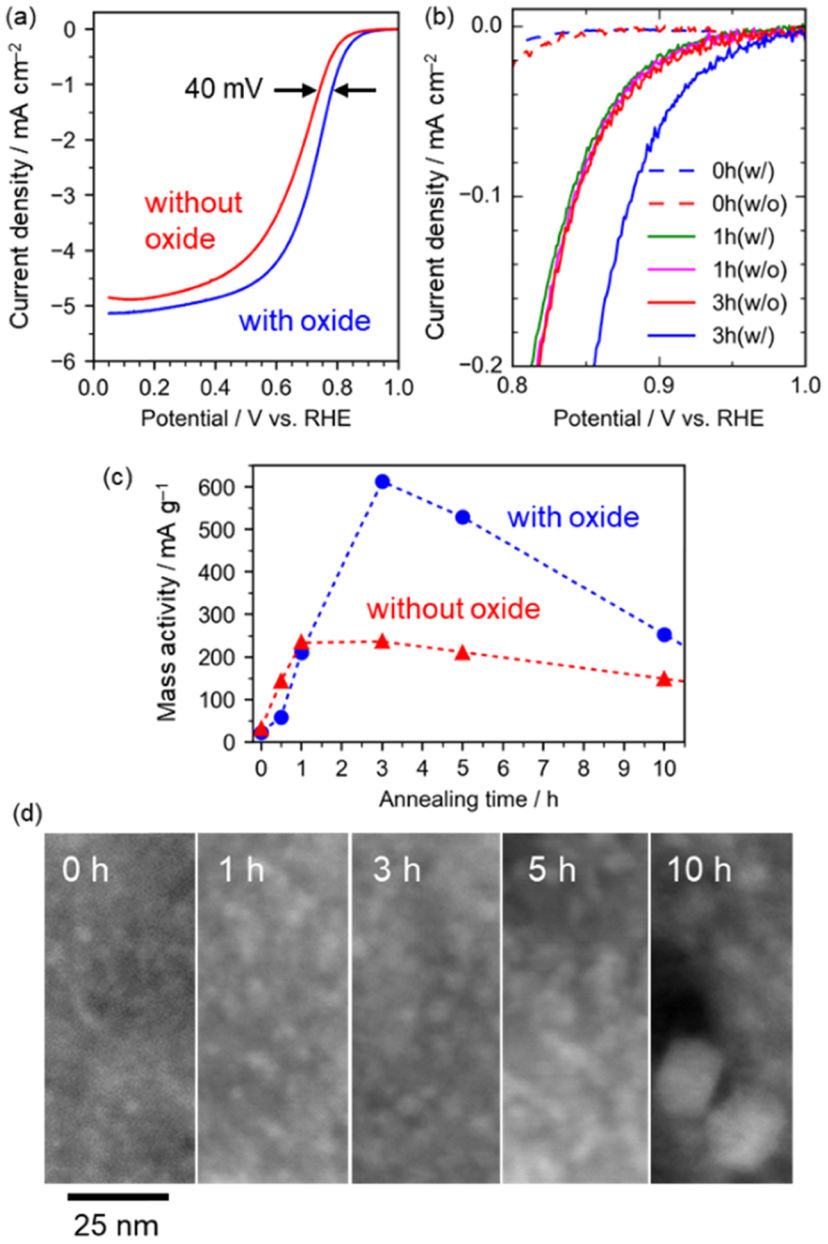

Figure 1. Electrochemical oxygen reduction activities of the catalysts annealed for a different retention time. The samples with (blue) and without (red) titanium oxides are compared. (a) Linear sweep voltammograms of the samples annealed for 3 h. The data were collected in 0.1 M H_2SO_4 (negative sweep) and then double-layer charge was corrected. The current densities are based on the geometric areas. (b) Comparison of kinetically controlled current densities. (c) Trend of mass activity of the samples annealed for a different retention time. The activities are normalized by the carbon contents. The activity was obtained at 0.80 V vs RHE. (d) High angle annular dark field scanning transmission electron microscopy images of the sample annealed for 0, 1, 3, 5, and 10 h (at the same magnification).

metric analysis (pyrolysis of TPPz molecules at 400−500 °C; pyrolysis of carbon nanotubes at 500−750 °C in dry air). Thus, the obvious particle growth observed at 10 h is probably due to the pyrolysis of the outer amorphous carbons, which results in particle growth on the external surface of the carbon matrix.

Electrochemical Measurements. The ORR activities were measured in an acidic electrolyte of 0.1 M H_2SO_4 using an electrochemical system with a rotating ring-disk electrode setup and a three-electrode cell (reference electrode is a reversible hydrogen electrode, RHE; counter electrode is a glassy carbon). The working electrode was a glassy carbon electrode coated with the samples (loading = 1.3−1.4 mg sample per cm^2; 4.90 ± 0.05 mg of the powder samples was dispersed in 160 μL of 1-hexanol with 8 μL of 5% Nafion, dropped onto the electrode, and then dried at 30 °C overnight).[9] We optimized this process to obtain a homogeneous and flat surface under an optical microscope. After cleaning the catalysts by scanning 200−400 cyclic voltammograms at 150 mV s^{-1} (0.05−1.2 V vs RHE), the voltammograms for the ORR test were obtained by scanning from 1.2 to 0.05 V vs RHE in an O_2-saturated electrolyte at 30 °C. The ORR activities were obtained by subtracting the double-layer charge obtained using a N_2-saturated electrolyte solution from the total current densities obtained using the O_2-saturated solution.

DOI: 10.1021/acsomega.7b00811
ACS Omega 2017, 2, 5209−5214

X-ray Structure Analysis. Pair distribution functions (PDFs) were obtained from the X-ray total scattering data collected using a Rigaku Rapid-S X-ray diffractometer with Ag Kα radiation (22 keV). The averaged wavelength, λ = 0.556 Å, was calculated using NIST CeO_2 standard by PDF fitting using the PDFgui program.[15] The samples were sealed in Lindeman glass capillaries. Twenty-four frames of the image data recorded on a curved imaging plate (exposure time = 2 h per frame) were integrated. After subtracting the image data collected without a sample, the intensity of each pixel was corrected for the proportion of Debye−Scherrer rings, thickness of the imaging plate, and polarization of X-ray; the pixel data were then converted into total scattering pattern. The intensities of the samples treated with HF and glass capillaries were subtracted from the scattering data of the samples with the oxides. These difference intensities are considered to contain the scattering from oxide phase as well as its interaction with the carbon phase, but the latter contribution was found to be negligible.[16] Thus, the total scattering patterns were normalized using the atomic scattering factors of TiO_x composition determined by the X-ray photoelectron spectroscopy (XPS) analyses, and the total structure function thus obtained was converted into the reduced PDFs by Fourier transformation.

The structures were analyzed by curve fitting of the PDFs using the PDFfit2 program[15] modified by adding an additional code for running the real-space reverse Monte Carlo simulations with bond-length restraints, bond-angle restraints, and atom swapping.[17]

Other Measurements. The XPS data were recorded using the Thermo Fisher Theta Probe using monochromatized Al Kα (1.487 keV) with charge neutralization. The spectra were corrected by the background subtraction with the Shirley method and charge-corrected using C 1s peak (284.5 eV). The peak intensities were determined by the least-squares curve fitting and converted into the atomic percentage using relative sensitivities. The high-resolution transmission electron microscopy (HR-TEM) images were obtained using a JEOL JEM-2100F high-resolution transmission electron microscope (HR-TEM) at 200 kV.

RESULTS AND DISCUSSION

Electrocatalytic Activity. Figure 1a−c shows that the samples annealed for more than 2 h exhibit catalytic activity associated with the presence of titanium oxides and gradually decreases with further annealing. The titanate particles were deposited on a carbon matrix (Figures 1d and S1), which was formed by the pyrolysis of the organic ligand of the titanium complex and deposited on carbon nanotubes used as current collectors for the electrochemical tests. The titanate particle size was about 2 nm up to 5 h, and bulky particles were observed on the external surface of the carbon matrix in the sample annealed for 10 h (Figures 1d and S1).

We carefully evaluated the electrocatalytic activities associated with the oxide phases because the carbon matrix exhibited catalyst activity, as widely known[18−20] (Figure 1b), as well as conductivity supporting titanium oxides in the electrochemical measurements. Thus, to clarify the activity associated the titanium oxides, we prepared the samples without the oxides by removing titanate with HF. The activities up to 1 h are attributable to the carbon materials, whereas the difference in the catalyst activities between the samples with and without oxides shown in Figures 1 and S2 is attributable to the activities of the oxide particles. Note that the influence of the HF treatment on the carbon materials were confirmed to be negligible (Table S1, Figures S3−S5).

Elemental States. Elemental states of Ti ions are important to understand the origin of the activity,[21,22] and thus they were analyzed by core-level X-ray photoelectron spectroscopy (XPS). The Ti 2p spectra (Figures 2 and S6) show that the

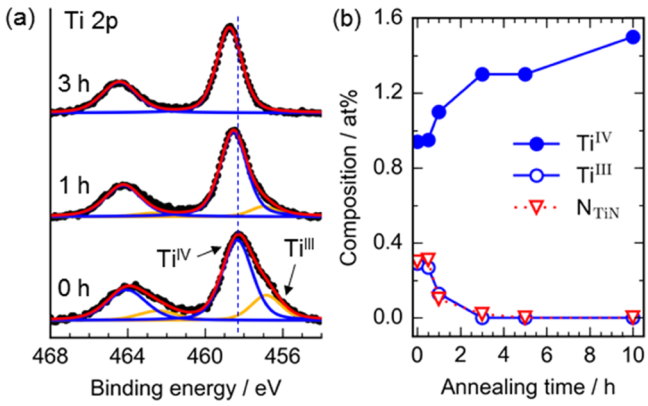

Figure 2. Elemental states of Ti ions analyzed using the core-level X-ray photoelectron spectra: (a) Ti 2p spectra. The black dots show the experimental data, the red curves are the simulated spectra, and other curves are fitted peaks of the Voigt functions. The vertical dotted line shows the position of the Ti^{IV} peak in the sample annealed for 0 h. (b) Composition change with annealing retention time.

samples annealed for less than 3 h contains Ti^{III} (456.8 eV) as well as Ti^{IV} (~458.5 eV).[23] Considering that the presence of similar amount of N state assignable to Ti−N (~396 eV) and that these two states synchronously decrease with annealing time (Figure 2b), the Ti^{III} state is attributable to the formation of Ti−N bonds (not titanium nitride). Because this Ti−N disappears at 3 h, the formation of Ti−N is not the origin of the ORR activity in this catalyst system. In addition to this oxidation, the Ti^{IV} peak shifted toward a higher binding energy with annealing retention time (Figure 2a; 458.3 eV at 0 h, 458.5 at 1 h, 458.7 at 3 and 5 h, and 458.8 eV at 10 h), indicating the core holes in Ti ions are less shielded in the more annealed samples. This corresponds to an elongation of the Ti−O bonding by structural transformation revealed by the following structure analysis. Thus, it is reasonable to consider the structural transformation occurring between 1 and 3 h is the key to understand the abrupt increase in the activity.

Atomic Structures. We analyzed their atomic structures by using the X-ray pair distribution functions (PDFs), which can inform us of the structures of all of the materials, even nanocrystals and amorphous materials, which can show broad features in the X-ray diffraction (XRD) patterns.[16] Figures 3 and S7 show that a structural transformation occurs from 1 to 3 h. This is consistent with the trend of the catalytic activity and the XPS results. It is apparent that the structural transformation is the key to understand the activity. Thus, in the following paragraphs, we discuss the structures in detail.

The structure of the sample annealed just by increasing the temperature up to 900 °C (retention time = 0 h) was found to be a lepidocrocite-type layered titanate. The formation of lepidocrocite-type titanate is not surprising because it was also reported as an intermediate in solvothermal reactions,[5] and the structure is apparently different from the "amorphous" titania prepared by the hydrolysis of titanium complex.[24] The stacking of the layers was disordered as indicated by the presence of the

DOI: 10.1021/acsomega.7b00811
ACS Omega 2017, 2, 5209−5214

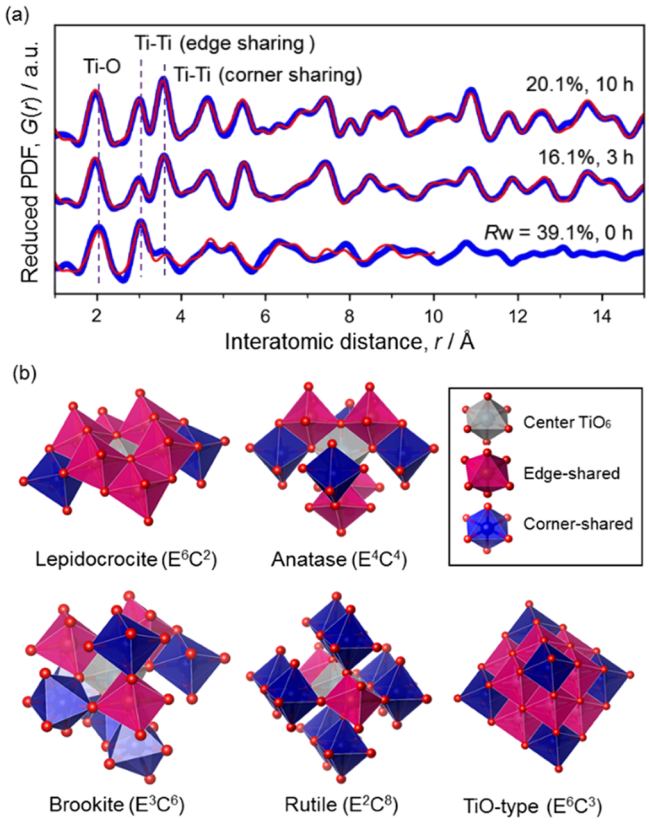

Figure 3. X-ray PDF structure analysis. (a) Pair distribution functions (Q_{max} = 17.5 Å^{-1}). The experimental data (blue) were fitted with simulated curves (red) based on structure models: (i) lepidocrocite-type TiO_2 (0 h), (ii) rutile and brookite (3 h), and (iii) rutile, brookite, and TiO-type structure (10 h). The fitting range was 1−10 Å for 0 and 1−20 Å for others. (b) Structure models and polyhedral connectivity. E^mC^n represents the polyhedral connectivity: numbers of edge sharing (E^m) and corner sharing (C^n).

diffuse scattering intensities located at below 9° in the XRD pattern (Figure S7a), which was assignable to the reflections along the interlayer direction. The PDF fitting model consisted of (i) an isolated layer for modeling chemical short-range order (i.e., atom positions in a layer) with two Ti atoms and four O atoms ($P2_1/m$) and (ii) three layers of the same lepidocrocite structures with large isotropic atomic displacement parameters for modeling number density.[5,25] Considering the little freedom of the modeling (note that the model had only one independent Ti site and O sites and did not include N or other defects such as Ti^{III} states), the modest fitting quality is enough for confirming the validity of this structure model. The modeled unit cell is a = 14.1(4) Å, b = 4.233(14) Å, c = 3.059(11) Å, and β = 88(4)°.

Upon the thermal treatment, the layered titanate was oxidized as revealed by the XPS analysis, and the absence of diffuse scattering associated with the stacking of the layers (<8°; Figure S7a) at 0.5 h suggests that the sintering of the layers has commenced, but its PDF is still almost unchanged (Figure S7b). The sample annealed for 1 h shows the XRD and PDF having the features of both samples annealed for 0.5 and 3 h, clearly indicating the commencement of the structural transformation, which may be triggered by the removal of nitrogen dopants (Figure 2b).[26] Through the transformation, the PDF peak reflecting the Ti−Ti distance in edge-shared linkage (∼3 Å) decreased, whereas the PDF peak reflecting that in corner-shared linkage (∼3.8 Å) increased. This is reasonable because lepidocrocite structure, wherein TiO_6 octahedra form a two-dimensional structure through edge-sharing connectivity, is rich in edge-shared linkage of TiO_6 octahedra (or denser) than the typical TiO_2 crystal structures (anatase, brookite, and rutile; Figure 3b).

To understand the structure of the sample annealed for 3 h, we tested a number of possible structure models of titanium oxides (e.g., rutile, anatase, brookite, etc.) with/without the defects analyzed by curve fitting of the PDFs using the PDFfit2 program[15] modified by adding an additional code for running the real-space reverse Monte Carlo simulations with bond-length restraints, bond-angle restraints, and atom swapping,[17] and finally found that large rutile particles (6.0(15) nm, 46 wt %; $P4_2/mnm$, a = 4.610(7) Å, c = 2.969(6) Å) and particles having brookite-like octahedral linkage (diameter = 2.2(3) nm, 54 wt %; $Pbca$, a = 9.21(6) Å, b = 5.28(3) Å, c = 5.49(3) Å) were formed. The formation of these structures from lepidocrocite-type titanate is reasonable in the light of the similar connectivity.[5,27] The formation of rutile crystals can be confirmed by XRD (Figure S7a) as well as TEM (Figure 4a), but brookite "crystals" were not found by the XRD and the TEM. Looking closely at the partial PDFs (Figure S8), the PDF fitted with brookite structure model indicates that the structure has (i) a short-range order within ca. 2 nm and (ii) more edge-shared TiO_6 octahedra than rutile (but less than lepidocrocite) (cf. Figure 3b).

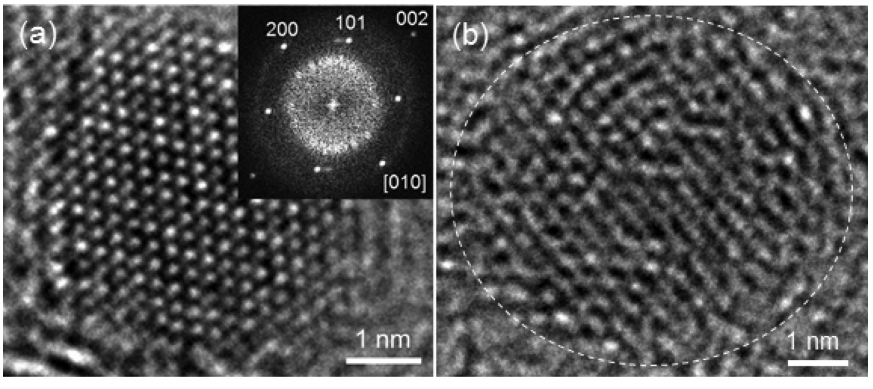

Figure 4. Bright-field HR-TEM images of titanium oxide particles in the sample annealed for 3 h. (a) A crystalline particle observed on the edge of the carbon matrix. The inset is a fast Fourier transform (FFT) image, which is assignable to the observation of rutile particle along [010]. (b) A modestly ordered particle (not assignable to rutile).

DOI: 10.1021/acsomega.7b00811
ACS Omega 2017, 2, 5209−5214

High-resolution transmission microscopy (HR-TEM) images enable us to distinguish if the domains are brookite nanocrystals or particles having short-range orders of such a linkage. The oxide particles on the edge of the carbon matrix are several nanometer scale and mostly show well-crystalline atomic-resolution images (Figure 4a), which are assignable to rutile TiO_2. We found that well-crystalline large rutile particles were also formed on the external surface of the carbon matrix in the sample annealed for 10 h. The other particles apart from the carbon edge appear to be not crystalline (Figure 4b), though the particle size is similar to the size of the rutile particles. We can observe local orders in these particles (Figure 4b), but an FFT analysis of these particles did not show clear spots, that is, no long-range orders existing in these particles. Thus, the ca. 2 nm scale domain found by PDF indicates averaged short-range orders in these particles. This lack of crystallinity of the brookite-like structure might be reasonable because brookite needs longer range orders to crystallize, that is, typical unit cell volumes of brookite (ca. 257 $Å^3$), rutile (ca. 62 $Å^3$), and anatase (ca. 136 $Å^3$). Alternatively, it might be due to the nanosize/morphology effect.[28]

Further annealing grew the particles located on the external surface of the carbon matrix (by TEM), which are well-crystalline rutile (47 wt % at 5 h and 46.7 wt % at 10 h) as described above. Note that the X-ray crystallite sizes for these samples (4.7(7) nm at 5 h and 3.8(3) nm at 10 h) seem inaccurate due to the narrower PDF fitting range (up to 2 nm), correlation of parameters in the three phases, and beam profile of the X-ray scattering measurements. Alternatively, as observed in the HR-TEM images (Figure S9), these results may reflect the formation of shear planes (or ordered defect sites) in the rutile structure. The content of rutile phase is constant from 3 to 10 h, though the size observed by the TEM increased, indicating the segregation and growth of rutile particles. That is, the smaller particles deposited in the carbon matrix were not transformed into rutile yet. This can be accounted for by the size effect (namely, because rutile has a large surface energy, extremely small rutile particles are not stable).[26]

PDF analysis (Figure S6) revealed that the content of the brookite-like domains decreased from 3 to 10 h (2.8(5) nm, 38.8 wt % at 5 h; 2.8(6) nm, 29.1 wt % at 10 h), whereas another phase assignable to a TiO-like cubic structure (modeled with the space group of $Fm\bar{3}m$, Ti occupancy = 0.5) was grown from 5 h (2.4(10) nm, 14.1 wt % at 5 h; 4.4(11) nm, 24.2 wt % at 10 h). This phase has the closest packing of oxygen ions and isotropic structure, and thus is reasonable to be formed by relaxing the oxygen packing of lepidocrocite-type structure. The averaged polyhedral connectivity of this phase is E^6C^3 as shown in Figure 3b (half of $E^{12}C^6$ in TiO because of the occupancy of Ti sites). The PDF of this additional phase is similar to that of the lepidocrocite-type structure (Figure S8) but slightly richer in the edge-sharing linkages of TiO_6 (Figure 3b) and longer Ti−O distance (Figure S8). Considering the absence of this phase at 3 h as well as their sizes and contents, this additional phase should be formed from the brookite-like phase, as clearly illustrated in Figure 5, and inactive in the oxygen reduction reactions.

CONCLUSIONS

The formation of a noncrystalline structure consisting of brookite-like TiO_6 octahedral linkages should be the origin of the catalytic activity in the electrochemical oxygen reduction reactions. Our investigations clearly show that the presence of a Ti^{III} state and a Ti−N do not account for the catalyst activity, though they may contribute to the formation of the brookite-like domains by stabilizing the lepidocrocite-type structure at the initial stage of the annealing process. We believe that such an octahedral network existing in the brookite-like domains contains active sites for the oxygen reduction reactions; however, honestly, the tiny rutile crystals (2−4 nm, found by TEM; Figure 4a) formed at 3 h may be another possible active structure in the oxygen reduction reactions and their particle growth resulted in a decrease in the activity. Currently, further investigations are being carried out to conclude this finding, which indicates the abrupt increase in the catalyst activity is probably attributable to the formation of such a noncrystalline phase in the structural transformation.

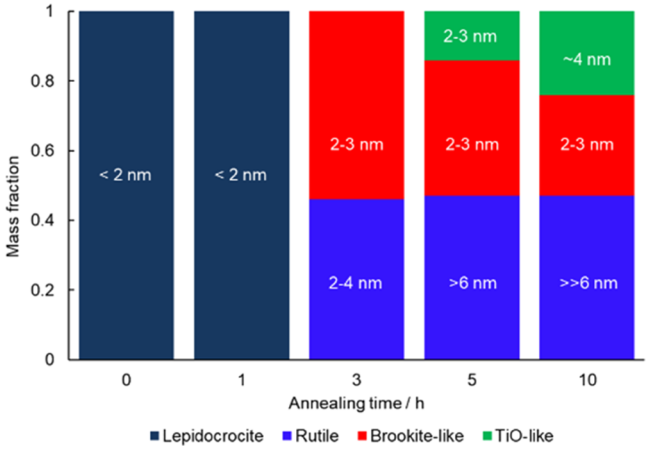

Figure 5. Summary of phase information. The numbers on the bars are the domain sizes determined by the PDF analysis, except the rutile particle sizes in the samples annealed for 5 and 10 h, which were observed by TEM observation. Details are discussed in the main text.

ASSOCIATED CONTENT

Supporting Information

The Supporting Information is available free of charge on the ACS Publications website at DOI: 10.1021/acsomega.7b00811.

Detailed information regarding the experimental methods, additional electrochemical data, XPS data, and PDF data (PDF)

AUTHOR INFORMATION

Corresponding Authors

*E-mail: TOMINAKA.Satosh@nims.go.jp (S.T.).
*E-mail: ishihara-akimitsu-nh@ynu.ac.jp (A.I.).

ORCID

Satoshi Tominaka: 0000-0001-6474-8665

Notes

The authors declare no competing financial interest.

ACKNOWLEDGMENTS

This work was in part supported by World Premier International Research Center (WPI) Initiative on Materials Nanoarchitectonics from MEXT, Japan, and by Grant-in-Aid for Scientific Research C (15K04614) from JSPS, Japan, and Development of Advanced PEFC Utilization Technologies/Development of Fundamental Technologies for PEFC Promotion from NEDO, Japan. The authors thank Orient Chemical Industries Co., Ltd., for supplying TiOTPPz. This

DOI: 10.1021/acsomega.7b00811
ACS Omega 2017, 2, 5209−5214

work was conducted under the auspices of the MEXT Program for Promoting the Reform of National Universities.

REFERENCES

(1) Dachille, F.; Simons, P. Y.; Roy, R. Pressure-temperature studies of anatase, brookite, rutile and TiO_2-II. *Am. Mineral.* **1968**, *53*, 1929−1939.
(2) Cox, P. A. *Transition Metal Oxides: An Introduction to Their Electronic Structure and Properties*; Oxford University Press, 2010; pp 294.
(3) Kaur, K.; Singh, C. V. Amorphous TiO_2 as a Photocatalyst for Hydrogen Production: A DFT Study of Structural and Electronic Properties. *Energy Procedia* **2012**, *29*, 291−299.
(4) Rino, J. P.; Studart, N. Structural correlations in titanium dioxide. *Phys. Rev. B: Condens. Matter Mater. Phys.* **1999**, *59*, 6643−6649.
(5) Gateshki, M.; Yin, S.; Ren, Y.; Petkov, V. Titania polymorphs by soft chemistry: Is there a common structural pattern? *Chem. Mater.* **2007**, *19*, 2512−2518.
(6) Tominaka, S.; Yoshikawa, H.; Matsushita, Y.; Cheetham, A. K. Topotactic reduction of oxide nanomaterials: unique structure and electronic properties of reduced TiO_2 nanoparticles. *Mater. Horiz.* **2014**, *1*, 106−110.
(7) Tominaka, S. Topotactic Reduction Yielding Black Titanium Oxide Nanostructures as Metallic Electronic Conductors. *Inorg. Chem.* **2012**, *51*, 10136−10140.
(8) Ishihara, A.; Hamazaki, M.; Arao, M.; Matsumoto, M.; Imai, H.; Kohno, Y.; Matsuzawa, K.; Mitsushima, S.; Ota, K. Titanium-Niobium Oxides Mixed with Ti_4O_7 as Precious-Metaland Carbon-Free Cathodes for Polymer Electrolyte Fuel Cells. *J. Electrochem. Soc.* **2016**, *163*, F603−F609.
(9) Hayashi, T.; Ishihara, A.; Nagai, T.; Arao, M.; Imai, H.; Kohno, Y.; Matsuzawa, K.; Mitsushima, S.; Ota, K. Temperature dependence of oxygen reduction mechanism on a titanium oxide-based catalyst made from oxy-titanium tetra-pyrazino-porphyrazine using carbon nano-tubes as support in acidic solution. *Electrochim. Acta* **2016**, *209*, 1−6.
(10) Hamazaki, M.; Ishihara, A.; Kohno, Y.; Matsuzawa, K.; Mitsushima, S.; Ota, K. Durability of Titanium-niobium Oxides Mixed with Ti_4O_7 as Non-precious-and Carbon-free Cathodes for PEFCs in H_2SO_4 at 80 degrees C. *Electrochemistry* **2015**, *83*, 817−819.
(11) Tominaka, S. Facile synthesis of nanostructured reduced titanium oxides using borohydride toward the creation of oxide-based fuel cell electrodes. *Chem. Commun.* **2012**, *48*, 7949−7951.
(12) Pei, D. N.; Gong, L.; Zhang, A. Y.; Zhang, X.; Chen, J. J.; Mu, Y.; Yu, H. Q. Defective titanium dioxide single crystals exposed by high-energy {001} facets for efficient oxygen reduction. *Nat. Commun.* **2015**, *6*, No. 8696.
(13) Baez, V. B.; Graves, J. E.; Pletcher, D. The Reduction of Oxygen on Titanium-Oxide Electrodes. *J. Electroanal. Chem.* **1992**, *340*, 273−286.
(14) Hayashi, T.; Ishihara, A.; Uehara, N.; Kohno, Y.; Matsuzawa, K.; Mitsushima, S.; Ota, K. Kinetic Study of Oxygen Reduction Reaction in Acid Solution Using Titanium Oxide-based Catalysts Prepared from Oxy-titanium Tetra-pyrazino-porphyrazine. *Electrochemistry* **2015**, *83*, 807−809.
(15) Farrow, C. L.; Juhas, P.; Liu, J. W.; Bryndin, D.; Bozin, E. S.; Bloch, J.; Proffen, T.; Billinge, S. J. L. PDFfit2 and PDFgui: computer programs for studying nanostructure in crystals. *J. Phys.: Condens. Matter* **2007**, *19*, No. 335219.
(16) Egami, T.; Billinge, S. J. L. *Underneath the Bragg Peaks: Structural Analysis of Complex Materials*; Elsevier: Oxford, U.K., 2003.
(17) Tominaka, S.; Kawakami, K.; Fukushima, M.; Miyazaki, A. Physical Stabilization of Pharmaceutical Glasses Based on Hydrogen Bond Reorganization under Sub-T_g Temperature. *Mol. Pharmaceutics* **2017**, *14*, 264−273.
(18) Guo, D.; Shibuya, R.; Akiba, C.; Saji, S.; Kondo, T.; Nakamura, J. Active sites of nitrogen-doped carbon materials for oxygen reduction reaction clarified using model catalysts. *Science* **2016**, *351*, 361−365.
(19) Zitolo, A.; Goellner, V.; Armel, V.; Sougrati, M. T.; Mineva, T.; Stievano, L.; Fonda, E.; Jaouen, F. Identification of catalytic sites for oxygen reduction in iron- and nitrogen-doped graphene materials. *Nat. Mater.* **2015**, *14*, 937−942.
(20) Lefvre, M.; Proietti, E.; Jaouen, F.; Dodelet, J. P. Iron-Based Catalysts with Improved Oxygen Reduction Activity in Polymer Electrolyte Fuel Cells. *Science* **2009**, *324*, 71−74.
(21) Chisaka, M.; Ando, Y.; Itagaki, N. Activity and durability of the oxygen reduction reaction in a nitrogen-doped rutile-shell on TiN-core nanocatalysts synthesised via solution-phase combustion. *J. Mater. Chem. A* **2016**, *4*, 2501−2508.
(22) Ishihara, A.; Tamura, Y.; Chisaka, M.; Ohgi, Y.; Kohno, Y.; Matsuzawa, K.; Mitsushima, S.; Ota, K. Titanium-Niobium Oxides as Non-Noble Metal Cathodes for Polymer Electrolyte Fuel Cells. *Catalysts* **2015**, *5*, 1289−1303.
(23) Moulder, J. F.; Stickle, W. F.; Sobol, P. E.; Bomben, K. D. *Handbook of X-ray Photoelectron Spectroscopy*; Physical Electronics, Inc.: MN, 1992.
(24) Zhang, H.; Chen, B.; Banfield, J. F.; Waychunas, G. A. Atomic structure of nanometer-sized amorphous TiO_2. *Phys. Rev. B: Condens. Matter Mater. Phys.* **2008**, *78*, No. 214106.
(25) Tominaka, S.; Hamoudi, H.; Suga, T.; Bennett, T. D.; Cairns, A. B.; Cheetham, A. K. Topochemical conversion of a dense metal-organic framework from a crystalline insulator to an amorphous semiconductor. *Chem. Sci.* **2015**, *6*, 1465−1473.
(26) Hanaor, D. A. H.; Sorrell, C. C. Review of the anatase to rutile phase transformation. *J. Mater. Sci.* **2011**, *46*, 855−874.
(27) Ozawa, T. C.; Sasaki, T. An Alkali-Metal Ion Extracted Layered Compound as a Template for a Metastable Phase Synthesis in a Low-Temperature Solid-State Reaction: Preparation of Brookite from $K_{0.8}Ti_{1.73}Li_{0.27}O_4$. *Inorg. Chem.* **2010**, *49*, 3044−3050.
(28) Pradhan, S. K.; Mao, Y.; Wong, S. S.; Chupas, P.; Petkov, V. Atomic-scale structure of nanosized titania and titanate: Particles, wires, and tubes. *Chem. Mater.* **2007**, *19*, 6180−6186.

DOI: 10.1021/acsomega.7b00811
ACS Omega 2017, 2, 5209−5214